ISSN 1674-1056
http://cpb.iphy.ac.cn
http://iopscience.iop.org/cpb
中国物理 B
Chinese Physics
中国物理
Chinese Physics B

On the nonclassical dynamics of cavityassisted fourchannel nonlinear coupler

Rafael Julius, Abdel-Baset M A Ibrahim, Pankaj Kumar Choudhury, Hichem Eleuch

Citation: Chin. Phys. B . 2018, 27(11): 114206. **doi:** 10.1088/1674-1056/27/11/114206

Journal homepage: http://cpb.iphy.ac.cn; http://iopscience.iop.org/cpb

What follows is a list of articles you may be interested in

Entangling two oscillating mirrors in an optomechanical system via a flying atom

Yu-Bao Zhang(张玉宝), Jun-Hao Liu(刘军浩), Ya-Fei Yu(於亚飞), Zhi-Ming Zhang(张智明)

Chin. Phys. B . 2018, 27(7): 074209. **doi:** 10.1088/1674-1056/27/7/074209

Estimation of photon counting statistics with imperfect detectors

Xiao-Chuan Han(韩晓川), Dong-Wei Zhuang(庄东炜), Yu-Xuan Li(李雨轩), Jun-Feng Song(宋俊峰), Yong-Sheng Zhang(张永生)

Chin. Phys. B . 2018, 27(7): 074208. **doi:** 10.1088/1674-1056/27/7/074208

Multi-window transparency and fast-slow light switching in a quadratically coupled optomechanical system assisted with three-level atoms

Wan-Ying Wei(魏晚迎), Ya-Fei Yu(於亚飞), Zhi-Ming Zhang(张智明)

Chin. Phys. B . 2018, 27(3): 034204. **doi:** 10.1088/1674-1056/27/3/034204

Generation of a squeezed state at 1.55 μ with periodically poled $LiNbO_3$

Liu Qin, Feng Jin-Xia, Li Hong, Jiao Yue-Chun, Zhang Kuan-Shou

Chin. Phys. B . 2012, 21(10): 104204. **doi:** 10.1088/1674-1056/21/10/104204

Demonstrating additional law of relativistic velocities based on squeezed light

Yang Da-Bao, Li Yan, Zhang Fu-Lin, Chen Jing-Ling

Chin. Phys. B . 2012, 21(7): 074201. **doi:** 10.1088/1674-1056/21/7/074201

On the nonclassical dynamics of cavity-assisted four-channel nonlinear coupler

Rafael Julius[1,2], Abdel-Baset M A Ibrahim[1,†], Pankaj Kumar Choudhury[3], and Hichem Eleuch[4,5]

[1] *Faculty of Applied Sciences, Universiti Teknologi MARA (UiTM), 40450 Shah Alam, Selangor, Malaysia*
[2] *Faculty of Applied Sciences, Universiti Teknologi Mara (UiTM) Perak, Tapah Campus, 35400 Tapah Road, Perak, Malaysia*
[3] *Institute of Microengineering and Nanoelectronics, Universiti Kebangsaan Malaysia, 43600 UKM Bangi, Selangor, Malaysia*
[4] *Department of Applied Sciences and Mathematics, College of Arts and Sciences, Abu Dhabi University, Abu Dhabi, United Arab Emirates*
[5] *Institute for Quantum Science and Engineering, Texas A&M University, College Station, Texas 77843, USA*

(Received 28 February 2018; revised manuscript received 3 August 2018; published online 25 October 2018)

The non-classical properties of light propagating in four-channel Kerr waveguides, confined in an optical cavity, are studied. The solution to the Hamiltonian of field operators is obtained semi-analytically by using symmetrically ordered phase-space representation. Full quantum analysis of the input coherent fields displays a strong transition of photon property between the super-Poissonian and sub-Poissonian statistics. It is found that the cavity-assisted multichannel system exhibits enhanced squeezing both in single- and compound-mode. This multichannel system may be utilized as an efficient quantum-light generator.

Keywords: squeezed states, Kerr effects, Langevin equation

PACS: 42.50.–p, 05.10.Gg, 42.65.–k, 42.82.Et **DOI:** 10.1088/1674-1056/27/11/114206

1. Introduction

Nowadays, computational applications are based on conventional electronic circuits, as extracted from the silicon technology. To meet the overwhelming demand for faster computers, the number of transistors confined in microprocessors has been doubling in capacity every two years,[1] and this pace would possibly make the measures (of the number of required transistors) to be on the atomic scale in the future. However, transistors, being a classical electronic component, introduce difficulties in attaining circuit features on the atomic scale. Optical quantum computer,[2] however, offers a way out with potential to deliver processing tasks much faster than the conventional ones. While squeezing cannot directly increase the storage capacity of the computer, within the context of phase estimation, quadrature noise squeezing remains advantageous, and the use of squeezed light would play an important role for future applications in optical computers.[3] Also, the squeezed light remains useful in many other promising applications, such as secured optical communication systems,[4] gravitational wave detectors,[5] precision measurements,[6] imaging,[7] and quantum information.[8] As such, in order to actualize squeezing for future applications, designing practical method of generating strong squeezing needs significant attention.

Rapid technological advancements in recent years allow strong squeezing to be generated in a number of nonlinear processes and quantum systems, e.g., parametric oscillators,[9–12] second harmonic generation,[13] atom–cavity couplings,[14–16] semiconductor microcavities,[17–19] optomechanical,[20–22] and nonlinear directional couplers (NLDC).[23–26] Systems having inherent fast nonlinear response, such as Kerr NLDC, however, possess the potential in generating strong squeezed light, especially when placed inside a cavity to resonantly amplify the nonlinearity. In addition, compared with other systems, Kerr NLDC is physically less complicated.[27]

In general, squeezing can be enhanced by direct manipulation of interaction among the modes of Kerr NLDC. This may be achieved by introducing either multimode single coupler[28–30] or multichannel single-mode configurations,[31] where the adjacent waveguides interact only with the central channel. Another practical approach would be confining the NLDC inside an optical cavity to resonantly amplify the nonlinearity.[32,33]

Quantum statistical properties of the cavity-assisted single coupler utilizing nonlinear waveguides have been theoretically investigated from the viewpoint of energy coupling[32] as well as the quantum dynamical effects.[34–37] Such configuration remains essential to improve squeezing in other devices, such as the degenerate-parametric amplifier.[37] In our previous work, we have reported the quantum properties of a multimode single coupler utilizing four-mode interaction with and without the aid of a cavity.[38] In such model,[38] the theory involves linear interaction between a single coherent mode in the first channel and three vacuum modes in the second channel.

The present paper aims to investigate the quantum dynamics of light modes (squeezing, in particular) propagating

†Corresponding author. E-mail: abdelbaset.ibrahim@gmail.com
© 2018 Chinese Physical Society and IOP Publishing Ltd

in a cavity-assisted multichannel NLDC, where four Kerr-like waveguides are engaged to form an eight-port coupler. The benefit of such configuration lies in achieving more versatile arrangement (of couplers) that allows easy control over the quantum correlations between modes. Moreover, the model presented here for the four-channel device gives a more adequate generalization of the traditional two-channel coupler system. In multimode waveguides, different modes propagate with different speeds, which makes it difficult to effectively estimate the generated squeezed states.[29] On the other hand, the use of single-mode waveguides contributes better flexibility in controlling the interaction (linear and nonlinear) between the guided modes and an effective estimation of the produced squeezed states of light.

In the newly proposed multichannel system, the squeezed states of light are observed in both quadrature components compared with the previously reported two-channel system where the squeezed light was observed in one of the quadrature components only.[26] The system under consideration appears to be a more efficient source of quantum light due to the evanescent field couplings of four interacting modes (instead of two, as in conventional two-waveguide coupler). To a significant extent, such quad-channel nonlinear coupler exhibits richer quantum effects due to the introduction of cavity, in addition to the involvement of the propagating fields in multimode interaction. Without accounting quantum fluctuations, the classical design of the system may find applications as essential elements in evanescent field optical sensing[39] and electro-optic switches.[40] For detailed design and other potential applications of multichannel directional coupler, see dissertation by McCosker.[41]

2. Design and modelling

The four-channel model of Kerr NLDC may be confined in an optical cavity by introducing partially reflecting mirrors (Fig. 1) at each end of the interacting waveguides;[32–38] this serves as a linear resonator. The use of a Kerr-like dielectric medium as optical waveguides provides an effective medium for multimode optical interaction due to the intensity-dependent Kerr effect. Another closely related nonlinear model, following an identical approach, implements the four-well Bose–Hubbard model with two different tunneling rates.[42] In Fig. 1, the guided mode in channel a_1 is prepared in the coherent state where the field E_1 is injected initially. Given that the neighboring waveguides are close enough to permit evanescent coupling, the energy from the coherent channel can be transferred to the neighboring vacuum waveguides a_2, a_3, and a_4. All the guided modes are assumed to be traveling in the same direction with constant phase and group velocities. Various physical quantities of the current system can be simulated by numerical means, as will be seen in the next section. The Hamiltonian describing the system is generally given by

$$\hat{H} = \hbar\left\{\hat{H}_{\text{system}} + \hat{H}_{\text{Kerr}} + \hat{H}_{\text{coupling}} + \hat{H}_{\text{pumping}} + \hat{H}_{\text{damping}}\right\}, \quad (1a)$$

where

$$\hat{H}_{\text{system}} = \omega \sum_{j=1}^{n} \hat{a}_j^{\dagger}\hat{a}_j, \quad (1b)$$

$$\hat{H}_{\text{Kerr}} = \left\{ g_a \sum_{j=1}^{n} \hat{a}_j^{\dagger 2}\hat{a}_j^2 + g_b \sum_{j=2}^{n} \hat{a}_1^{\dagger}\hat{a}_1\hat{a}_j^{\dagger}\hat{a}_j + g_c \sum_{j=3}^{n} \hat{a}_2^{\dagger}\hat{a}_2\hat{a}_j^{\dagger}\hat{a}_j + g_c\hat{a}_3^{\dagger}\hat{a}_3\hat{a}_4^{\dagger}\hat{a}_4 \right\}, \quad (1c)$$

$$\hat{H}_{\text{coupling}} = \left\{ k_1 \sum_{j=2}^{n} (\hat{a}_j^{\dagger}\hat{a}_1 + \hat{a}_1^{\dagger}\hat{a}_j) + k_2 \sum_{j=3}^{n} (\hat{a}_j^{\dagger}\hat{a}_2 + \hat{a}_2^{\dagger}\hat{a}_j) + k_2(\hat{a}_3^{\dagger}\hat{a}_4 + \hat{a}_4^{\dagger}\hat{a}_3) \right\}, \quad (1d)$$

$$\hat{H}_{\text{pumping}} = \mathrm{i} \sum_{j=1}^{n} \left\{ E_j\hat{a}_j^{\dagger} - E_j^{*}\hat{a}_j \right\}, \quad (1e)$$

$$\hat{H}_{\text{damping}} = \sum_{j=1}^{n} \left\{ \hat{a}_j\Gamma_j^{\dagger} + \hat{a}_j^{\dagger}\Gamma_j \right\}. \quad (1f)$$

In the system of Eqs. (1b)–(1f), $\hat{a}$ and $\hat{a}^{\dagger}$ are the bosonic creation and annihilation ladder operators, respectively. Equation (1b) describes the system Hamiltonian for each individual mode inside the four waveguides without interaction; for example, in the first waveguide, the mode is described by $\hat{H}_{1,\text{system}} = \hbar\omega\hat{a}_1^{\dagger}\hat{a}_1$. The coefficient ω is the operating frequency and $\hbar = h/2\pi$ is the reduced Planck constant. The Hamiltonian in Eq. (1c) represents the third-order Kerr effect which results from both self- and cross-action nonlinearities where g_a is the self-action nonlinear coupling constant, and g_b and g_c are the cross-action coupling constants with positive proportionality to the third-order susceptibility $\chi^{(3)}$. The Hamiltonian in Eq. (1d) represents the linear coupling between the modes in the adjacent waveguides due to the evanescent fields. The coefficient k is the linear coupling constant with the subscript 1 for the interaction between the mode a_1 with the other modes a_2, a_3, and a_4, and the subscript 2 for the interaction between a_2, a_3, and a_4, as shown in Fig. 1(b). The Hamiltonian in Eqs. (1e) and (1f) represents the inclusion of cavity in the system where H_{pumping} describes the pumping term derived from the classical driving field and H_{damping} describes the damping term due to the coupling with the heat bath. The cavity parameters comprised of Γ_{ch1}, Γ_{ch2}, Γ_{ch3}, and Γ_{ch4} are the operators representing cavity losses in each channel, while $\Gamma_{\text{ch1}}^{\dagger}$, $\Gamma_{\text{ch2}}^{\dagger}$, $\Gamma_{\text{ch3}}^{\dagger}$, and $\Gamma_{\text{ch4}}^{\dagger}$ are their respective conjugates. E denotes the coherent driving field.

It should be noted that figure 1 shows one possible configuration of four-channel waveguides placed in a cavity. The current configuration exactly matches the coupling Hamiltonian in Eq. (1d), where a single waveguide (a_1) can be set at the center with three other vacuum waveguides (a_2, a_3, and a_4)

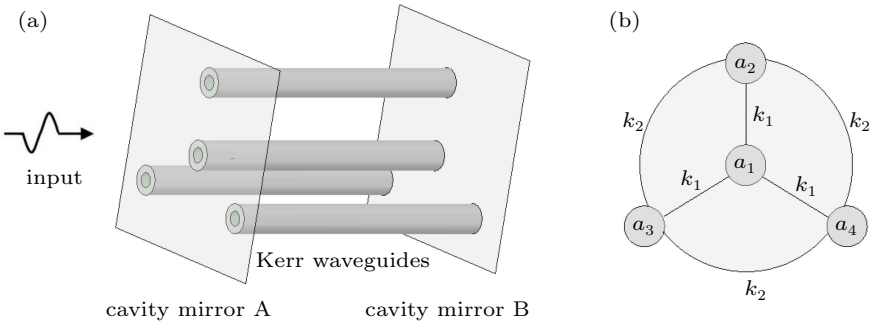


Fig. 1. Schematic diagram of a cavity-assisted four-channel directional coupler. (a) Complete structure. (b) Cross section.

in the surrounding. The coefficient k_1 refers to the interaction with the center waveguide, while k_2 gives the interaction among the surrounding ones. However, the arrangement of vacuum channels around the coherent channel is not unique. Nevertheless, regardless of which arrangement is followed, the separation distance among the vacuum waveguides remains almost identical. From Eq. (1), the master equation can be written as

$$\frac{\partial\hat{\rho}}{\partial t}=-\frac{\mathrm{i}}{\hbar}\left[\hat{H},\hat{\rho}\right]+\sum_{j=1}^{n}\gamma_j(2\hat{a}_j\hat{\rho}\hat{a}_j^{\dagger}-\hat{a}_j^{\dagger}\hat{a}_j\hat{\rho}-\hat{\rho}\hat{a}_j^{\dagger}\hat{a}_j), \quad (2)$$

with γ_j being the damping coefficient of modes. In Schrödinger picture, the time evolution equation for the reduced density matrix contains the heat bath coupling through the Liouvillian terms. To allow only the presence of quantum fluctuation, the coupling between laser modes and bath modes has been eliminated by assuming vanishing thermal fluctuation.

In the phase space, the operator equation is converted into a partial differential equation for the quasi probability function of the reduced density operator. In Wigner representation, the mean field is given by the expectation value of the symmetrically ordered ladder operator for single mode optical field basis $\langle\hat{a}_1^{\dagger}\hat{a}_1\rangle_{\text{symmetric}}$. This expectation value corresponds to the average of the complex variables such that $\langle\hat{a}_1^{\dagger}\hat{a}_1\rangle_{\text{symmetric}}=(\alpha_1^{*}\alpha_1)_{\text{average}}$, where α_1 and α_1^{*} are complex conjugate classical variables in the phase space. Applying a standard approach,[43] the master equation (2) may be mapped onto its equivalent stochastic differential equation in Wigner representation for $n=4$ to yield

$$\begin{aligned}\frac{\partial\alpha_1}{\partial\tau}=\Big\{&-\mathrm{i}\Delta_1\alpha_1-2\mathrm{i}g_a\left(|\alpha_1|^2-1\right)\alpha_1-\mathrm{i}k_1\left(\alpha_2+\alpha_3+\alpha_4\right)\\&-\mathrm{i}g_b\left(\alpha_1\alpha_2^{*}\alpha_2+\alpha_1\alpha_3^{*}\alpha_3+\alpha_1\alpha_4^{*}\alpha_4-\frac{3}{2}\alpha_1\right)\\&-\gamma_1\alpha_1+E_1+\sqrt{2\gamma_1}\eta_1(\tau)\Big\}, \quad (3a)\end{aligned}$$

$$\begin{aligned}\frac{\partial\alpha_2}{\partial\tau}=\Big\{&-\mathrm{i}\Delta_2\alpha_2-2\mathrm{i}g_a\left(|\alpha_2|^2-1\right)\alpha_2-\mathrm{i}k_1\left(\alpha_1+\alpha_3+\alpha_4\right)\\&-\mathrm{i}g_b\left(\alpha_2\alpha_1^{*}\alpha_1-\frac{3}{2}\zeta\alpha_2\right)-\mathrm{i}g_c\left(\alpha_2\alpha_3^{*}\alpha_3+\alpha_2\alpha_4^{*}\alpha_4\right)\\&-\gamma_2\alpha_2+E_2+\sqrt{2\gamma_2}\eta_2(\tau)\Big\}, \quad (3b)\end{aligned}$$

$$\begin{aligned}\frac{\partial\alpha_3}{\partial\tau}=\Big\{&-\mathrm{i}\Delta_3\alpha_3-2\mathrm{i}g_a\left(|\alpha_3|^2-1\right)\alpha_3-\mathrm{i}k_1\alpha_1-\mathrm{i}k_2\left(\alpha_2+\alpha_4\right)\\&-\mathrm{i}g_b\left(\alpha_3\alpha_1^{*}\alpha_1-\frac{3}{2}\zeta\alpha_3\right)-\mathrm{i}g_c\left(\alpha_3\alpha_2^{*}\alpha_2+\alpha_3\alpha_4^{*}\alpha_4\right)\\&-\gamma_3\alpha_3+E_3+\sqrt{2\gamma_3}\eta_3(\tau)\Big\}, \quad (3c)\end{aligned}$$

$$\begin{aligned}\frac{\partial\alpha_4}{\partial\tau}=\Big\{&-\mathrm{i}\Delta_4\alpha_4-2\mathrm{i}g_a\left(|\alpha_4|^2-1\right)\alpha_4-\mathrm{i}k_1\alpha_1-\mathrm{i}k_2\left(\alpha_2+\alpha_3\right)\\&-\mathrm{i}g_b\left(\alpha_4\alpha_1^{*}\alpha_1-\frac{3}{2}\zeta\alpha_4\right)-\mathrm{i}g_c\left(\alpha_4\alpha_2^{*}\alpha_2+\alpha_4\alpha_3^{*}\alpha_3\right)\\&-\gamma_4\alpha_4+E_4+\sqrt{2\gamma_4}\eta_4(\tau)\Big\}. \quad (3d)\end{aligned}$$

The quantum mechanical master equation (2) is converted to its equivalent classical system of Eq. (3) in two mathematical stages. First, the quantum-classical correspondence[43] in Wigner representation is used to convert Eq. (2) to a Fokker–Planck equation. In the process of deriving the Fokker–Planck equation, higher-order derivatives above the second-order are usually truncated, and the resulting Fokker–Plank equation is a good approximation to the original problem. Second, the Ito calculus is used to convert the Fokker–Planck equation to the equivalent system of Langevin stochastic Eq. (3). The variables α_j in this case are the classical complex number representations to that of bosonic operators for modes 1 to 4 in the propagation direction τ.

In these equations, $\Delta_j\,(j=1\text{–}4)$ represents detuning between the mode and cavity frequencies. The stochasticity of Eq. (3) is stipulated by the noise element $\eta_j(\tau)$ which, in turn, depends on the rate of photon losses γ_j. In order to obtain stable integration, equation (3) is scaled to the dimensionless form by introducing $\tau_{\text{s}}=k_1\tau$, $\Delta_{j\text{s}}=\Delta_j/k_1$, $\gamma_{j\text{s}}=\gamma_j/k_1$, $k_{1\text{s}}=k_1/k_1$, $k_{2\text{s}}=k_2/k_1$, $g_{(a,b,c)\text{s}}=g_{(a,b,c)}/k_1$, $E_{j\text{s}}=E_j/k_1$, and $\eta_{j\text{s}}(\tau)=\eta_j(\tau)/h^{1/2}$, where the subscript s refers to the scaled form of these coefficients and the parameter ζ is the

controlling variable responsible in tuning the cross-action nonlinear coupling. An estimation of the input parameter can be found in our previous work.[38] For realistic results, the input parameters used in the following section are adopted from the literature following Refs. [26], [28], [29], and [30] so that the scope remains consistent with the previous work in this area. The output fields may also be experimentally realized via standard detection schemes of direct photodetection and balanced homodyne detection.

3. Results and discussion

Here, we have observed that the non-classical properties are sensitive to the cavity detuning. We, therefore, restrict the detuning to lower values (i.e., $\Delta_{js} = 1$), high (i.e., $\Delta_{js} = 10$), and the resonance case (i.e., $\Delta_{js} = 0$). The classical driving force of $E_{1s} = 1$ is initialized in the first channel, and $E_{2s} = E_{3s} = E_{4s} = 0$ for the other channels. The first channel is sampled in the coherent state with the eigenvalue $\alpha_1 = 1$ and the other in the vacuum states with $\alpha_2 = \alpha_3 = \alpha_4 = 0$. The linear coupling coefficients are approximated at $k_{1s} = 1$, $k_{2s} = 0.5$, and the nonlinear self-action and cross-action coefficients are fixed at $g_{as} = 0.01$ and $g_{bs} = g_{cs} = 2g_{as}$ with small damping $\gamma_{js} = 0.001$ and $\zeta = 1$. The evanescent damping of coupling may lead to amplitude reduction of power transfer. Provided that the surface of waveguides is of high quality to prevent substantial energy loss, the self- and cross-action nonlinear coefficients may assume comparable spectral coupling.[25]

3.1. Time evolution of the mean field

In Wigner representation, the operator product is calculated in symmetrical order so that the ensemble average of photon number $\langle|\alpha|^2\rangle_W$ is given by $(1/2)\langle\alpha^\dagger\alpha + \alpha\alpha^\dagger\rangle$. Although certain approximation is used in the stochastic modeling for exact mapping of Fokker–Planck equation of the system, the results of Wigner representation remain feasible. At high detuning coefficient ($\Delta_{js} = 10$), slight amplification in the mean amplitude of oscillation, as shown in Fig. 2(a), is observed. The overall energy distribution in the coherent channel is rather erratic; nevertheless, stable energy transfer across all channels is visible. During the evanescent coupling, most of the energy is transferred to other guides, leaving behind some in the coherent channel. The transferred energy oscillates across the multichannel structure with the same distribution on each channel.

In Fig. 2(b), as a consequence of cavity amplification, the field amplitude is observed to be several times larger than its initial value. Such an effect is pronounced in the coherent channel where the mean field is scaled down to five times of its amplified value. The period of complete energy transfer is also longer than that simulated in the two-channel model,[26] which indicates that the propagation of energy across waveguides is slower due to the multichannel structure. An identical feature of oscillations is observed in the other channels as well with the energy being shared approximately equally among the waveguides.

For the case of equal operating frequencies (i.e., vanishing detuning with $\Delta_{js} = 0$), effects identical to that corresponding to the situation of $\Delta_{js} = 10$ are observed (Fig. 2(c)); in this case, the oscillation of amplitude amplification appears in all channels. In general, the dynamics of intracavity mean fields show a classical damping behavior over their respective interaction length before reaching the steady-state oscillation. The total energy oscillates back-and-forth across the system in all considered cases. Such effective periodical exchange of photons provides potentials for the transfer of quantum effects from one channel to another.

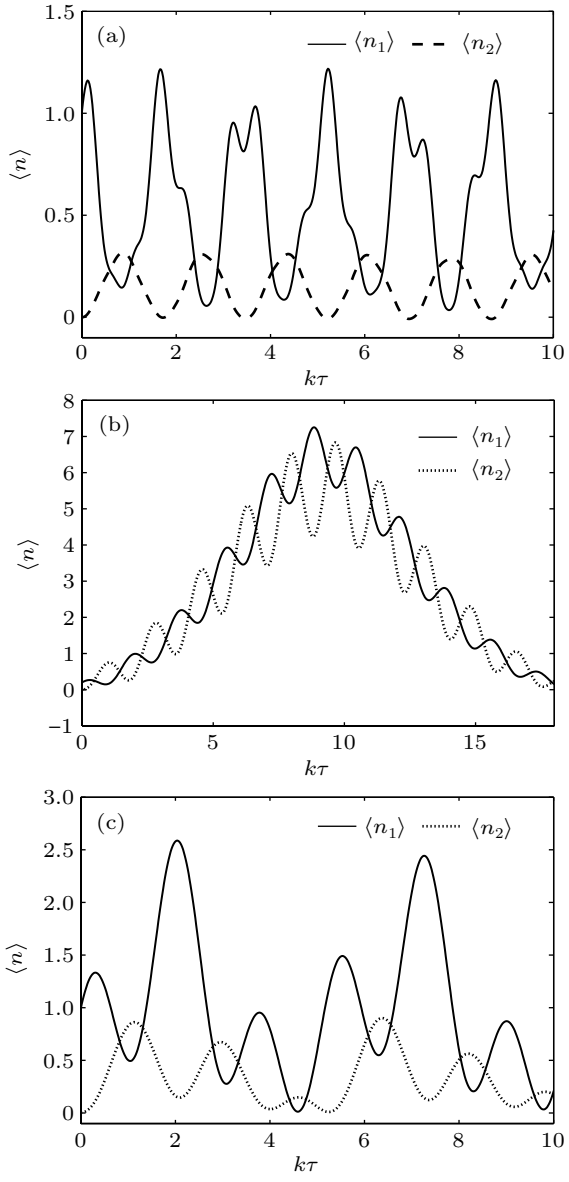


Fig. 2. The evolution of mean photon number in the coherent $\langle n_1\rangle$ and vacuum $\langle n_2\rangle$ channels with the input parameters (a) $\Delta_{js} = 10$, (b) $\Delta_{js} = 1$, and (c) $\Delta_{js} = 0$.

3.2. Sub-Poissonian photon statistics

A convenient way of characterizing the statistical distribution property of multichannel intracavity fields is to use Mandel Q parameter[44]

$$Q = \frac{(\Delta n')^2}{(n')} - 1, \tag{4}$$

where $(\Delta n')^2 = (n'^2) - (n')^2$ and $n' = \hat{a}^\dagger \hat{a}$. In Wigner representation, the symmetrical operator product of the number operator is given by

$$\left\langle \hat{a}^{\dagger x} \hat{a}^y \right\rangle_{\mathrm{W}} = \int \frac{\mathrm{d}^2\alpha}{\pi} W(\alpha, \alpha^*)\, \alpha^{*x}, \alpha^y. \tag{5}$$

Thus, for $x = y = 1, 2$, the number operator may be written as

$$\left\langle n' \right\rangle = \left\langle |\alpha|^2 \right\rangle_{\mathrm{W}} - \frac{1}{2}, \tag{6}$$

$$\left\langle n'^2 \right\rangle = \left\langle |\alpha|^4 \right\rangle_{\mathrm{W}} - \left\langle n' \right\rangle - \frac{1}{2}, \tag{7}$$

yielding

$$Q = \frac{\left\langle |\alpha|^4 \right\rangle_{\mathrm{W}} - \left\langle |\alpha|^2 \right\rangle_{\mathrm{W}}^2 - \left\langle |\alpha|^2 \right\rangle_{\mathrm{W}} + (1/4)}{\left\langle |\alpha|^2 \right\rangle_{\mathrm{W}} - (1/2)}. \tag{8}$$

A positive Q-value refers to the photon statistics as super-Poissonian following the classical interpretation, whereas a negative value of Q is associated with sub-Poissonian statistics of quantum phenomenon. In a photon-counting experiment, the intrinsic statistical nature of photons may be determined by analyzing the average photon arrival rate.

In Fig. 3(a), where the Q parameter is plotted against $k\tau\,(k = k_1)$ at $\Delta_{js} = 10$, the evolution of Q parameter in the coherent channel reveals fluctuating statistics to be of both the super-Poissonian and sub-Poissonian kinds. Coherent light adherent Poissonian statistics ($Q = 0$) usually relates to photons arriving at the photodetector in clusters. Thus, both the super-Poissonian and sub-Poissonian statistics give the merit of comparison whether they have larger or smaller property of photo-count noise than that of the Poisson distribution, provided that those are of the same intensity.

At $\Delta_{js} = 10$, photon statistical distribution of the system in the coherent channel can be either super-Poissonian or sub-Poissonian. It follows that for smaller detuning, such as $\Delta_{js} = 1$ (Fig. 3(b)), fluctuation of the Q parameter can be higher than the coherent light for some interval of interaction, especially when the system is initially launched. The system may also exhibit the sub-Poissonian property. For example, there appeared an obvious reduction of the photo-count noise at $k\tau \approx 7$. The highest peak of super-Poissonian is observed at $\Delta_{js} = 0$, as is shown in Fig. 3(c). However, a series of steep transitions to sub-Poissonian behavior occur at $k\tau \approx 4$ and $k\tau \approx 10$. It must be noted down that the negative value of Q may also relate to the existence of photon antibunching, provided that the time interval for detecting one arriving photon and another one at a later time is increasing.

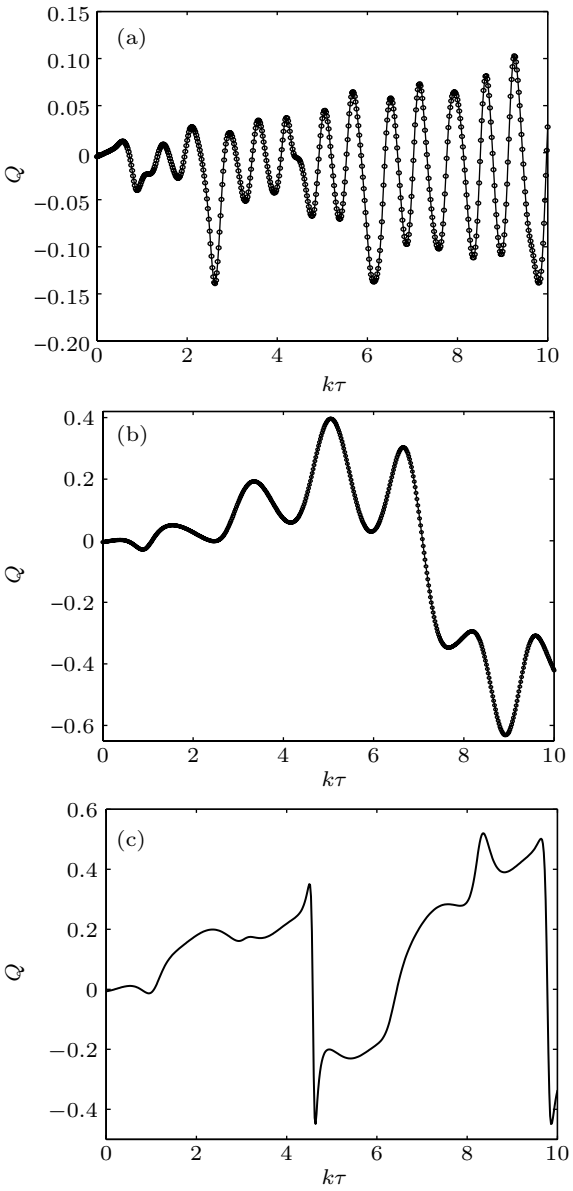


Fig. 3. The evolution of Q parameter in the coherent channel α_{c1} versus $k\tau$ with the input parameters (a) $\Delta_{js} = 10$, (b) $\Delta_{js} = 1$, and (c) $\Delta_{js} = 0$.

3.3. Squeezing

In quantum optical systems, the optical fields obey the laws of quantum mechanics, and thus, have an inherent quantum indeterminacy that cannot be removed. In the framework of single-mode basis, the field quadrature components are given by $X = 2^{-1/2}(\hat{a} + \hat{a}^\dagger)$ and $Y = -2^{-1/2}\mathrm{i}(\hat{a} - \hat{a}^\dagger)$.[45] The quadrature components X and Y obey the commutation relation $[X, Y] = \mathrm{i}$. In accordance with the Heisenberg uncertainty principle, the quadrature variances $(\Delta X)^2 = (X^2) - (X)^2$ and $(\Delta Y)^2 = (Y^2) - (Y)^2$ must satisfy $\Delta X \Delta Y \geq (1/2)$, so that the uncertainty principle is not violated. The squeezed

light emerges with quadrature properties $\langle(\Delta X)^2\rangle < (1/4)$ or $\langle(\Delta Y)^2\rangle < (1/4)$.[46] For compound-mode squeezing, the uncertainty relation yields

$$\langle(\Delta\hat{X}_j)^2\rangle\langle(\Delta\hat{Y}_j)^2\rangle \geq \frac{|c_j|^2}{16}, \tag{9}$$

where j takes the values 2, 3, and 4 for two-mode, three-mode, and four-mode, respectively. For a fair comparison, equation (9) may be rearranged to give squeezing expressions of the form[28]

$$S_{jx} = 4\langle(\Delta\hat{X}_j)^2\rangle - |c_j| \leq 0, \tag{10a}$$
$$S_{jy} = 4\langle(\Delta\hat{Y}_j)^2\rangle - |c_j| \leq 0, \tag{10b}$$

with $-S_{jx}$ being the quadrature squeezing in the X-component, whereas $-S_{jy}$ being that in the Y-component. For a single-mode squeezing, $j = 1$, so that $S_{1x} = 4\langle(\Delta X_1)^2\rangle - |C_1|$ with $C_1 = 1$. A similar definition may be given to the Y-quadrature component as well.

In Fig. 4(a), single-mode quadrature evolution is presented at detuning $\Delta_{js} = 10$. This figure shows squeezing with an interesting pattern of collapsed and revival in the coherent channel; similar features of oscillation can be obtained in the other channels as well. Squeezing occurs in both the X- and Y-quadrature components periodically, depending on the interaction length; it can be much lesser than the shot noise level, especially later in their evolution. In addition to squeezing in the system without cavity, the cavity-assisted system exhibits a swift squeezing oscillation. This, in turn, contributes to the enhancement of noise reduction in both the quadrature components (Fig. 4(b)). Since both the quadrature variances are oscillating in symmetrical pattern, the Y-quadrature is also subjected to the same impact.

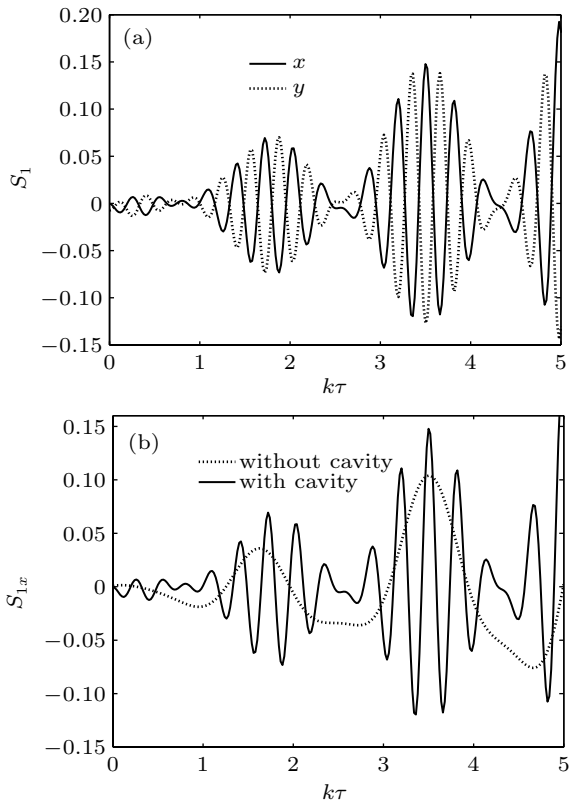


Fig. 4. The evolution of quadrature variances in the coherent channel α_{c1} with the detuning fixed at $\Delta_{js} = 10$. (a) Both quadrature variances S_{1x} and S_{1y}, and (b) comparison between the first quadrature variances S_{1x} with and without a cavity.

The numerical calculation of squeezing for detuning $\Delta_{js} = 1$ is shown in Fig. 5. It is observed that, at small detuning coefficient, squeezing occurs in all channels. Unlike the cases at $\Delta_{js} = 10$, squeezing at $\Delta_{js} = 1$ exhibits lower frequency of oscillation between the two quadrature components. Although detuning the cavity to $\Delta_{js} = 1$ eliminates swift oscillation pattern, the reduction of detuning remains advantageous in reducing the quantum noise. The comparison of both quadratures of the coherent channel between $\Delta_{js} = 10$ and $\Delta_{js} = 1$ (Fig. 5) shows maximal squeezing at $\Delta_{js} = 1$. The system with smaller detuning is found to be more capable of generating longer squeezing where the highest value appears at a maximal distance before reaching the steady-state oscillation.

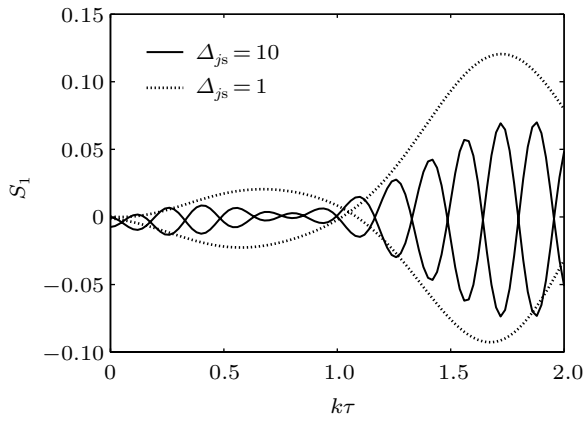


Fig. 5. Comparison of evolution for both quadrature variances S_{1x} and S_{1y} in the coherent channel α_{c1} at the detuning $\Delta_{js} = 10$ and $\Delta_{js} = 1$.

In the absence of mismatch between the operating frequencies (i.e., $\Delta_{js} = 0$), it is found that stronger squeezing (than that obtained corresponding to $\Delta_{js} = 10$ and $\Delta_{js} = 1$) is possible. Figure 6 illustrates the comparison of squeezing features corresponding to the detuning coefficients $\Delta_{js} = 1$ and $\Delta_{js} = 0$. The case of zero detuning also results in the disappearance of the leaf-revival-collapse-like squeezing; much lower frequency of oscillation occurs in this case. Nevertheless, squeezing with better reduction of uncertainties product emerges periodically between the two oscillating quadrature components. While similar effect is also observed in the other channels, squeezing becomes maximum in the coherent channel.

To account for compound-mode squeezing, the interaction between the waveguides may be reduced so that the system interaction remains limited between the vacuum and

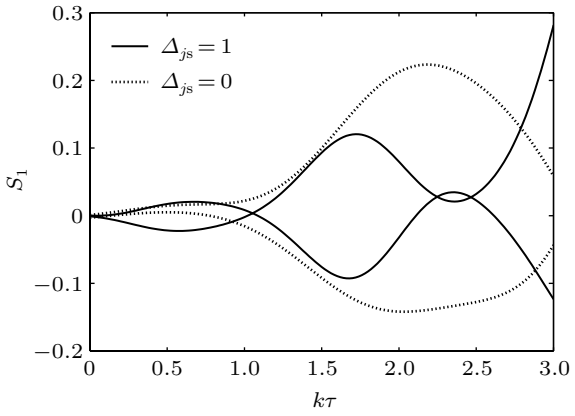


Fig. 6. Comparison of evolution for both quadrature variances S_{1x} and S_{1y} in the coherent channel α_{c1} at the detuning $\Delta_{js}=1$ and $\Delta_{js}=0$.

coherent channels only, while all the vacuum channels are isolated from each other. The mechanism is easily manifested by setting $k_{2s}=0$ and $\zeta=1/3$ in Eq. (3). Also, we focus only on the highest compound-mode squeezing of the first-order basis where the effect is maximal by setting $j=4$ in Eq. (10). Figure 7(a) gives the X-quadrature evolution of the coherent channel for both single-mode S_{1x} and four-mode S_{4x} quadrature. Launching the system at $\Delta_{js}=0$ results in quadrature squeezing with a strong oscillatory behavior of collapsed-and-revival pattern. It is to be noted that the maximal squeezing of single-mode may be improved following the previous arrangement where all the vacuum modes are allowed to couple with each other. With all the vacuum modes being isolated (as in the present case), the result predicted in four-mode basis shows a tendency of generating stronger squeezing limit than that exhibited in the single-mode.

In Fig. 7(b), we compare the dynamics of both the quadrature variances in the coherent channel for single-mode S_{1x}, S_{1y} and four-mode S_{4x}, S_{4y} at $\Delta_{js}=1$. Within the considered interaction length, the quantum noise between the two quadrature components of the single-mode field is uniformly distributed, and squeezing is generated alternatingly between the quadrature obeying the uncertainty rule. The maximal squeezing is also found to be generated at the maximal distance. As one would hope to achieve for the multichannel system, the compound-mode squeezing at $\Delta_{js}=1$ exemplifies even stronger squeezing. Identical to the single-mode squeezing, symmetrical noise distribution between the two quadrature components also appears in the compound mode. However, the maximal squeezing does not necessarily depend on the interaction length, as illustrated in Fig. 7(b); a sudden peak of noise reduction may appear, for example at $k\tau=1, 2.5$.

We further investigate the possible existence of single-mode S_{1x}, S_{1y}, and four-mode S_{4x}, S_{4y} squeezing by simulating the system equation at zero detuning. A comparison between quadrature evolutions in the coherent channel is depicted in Fig. 7(c). As shown, the perfect matching between the two

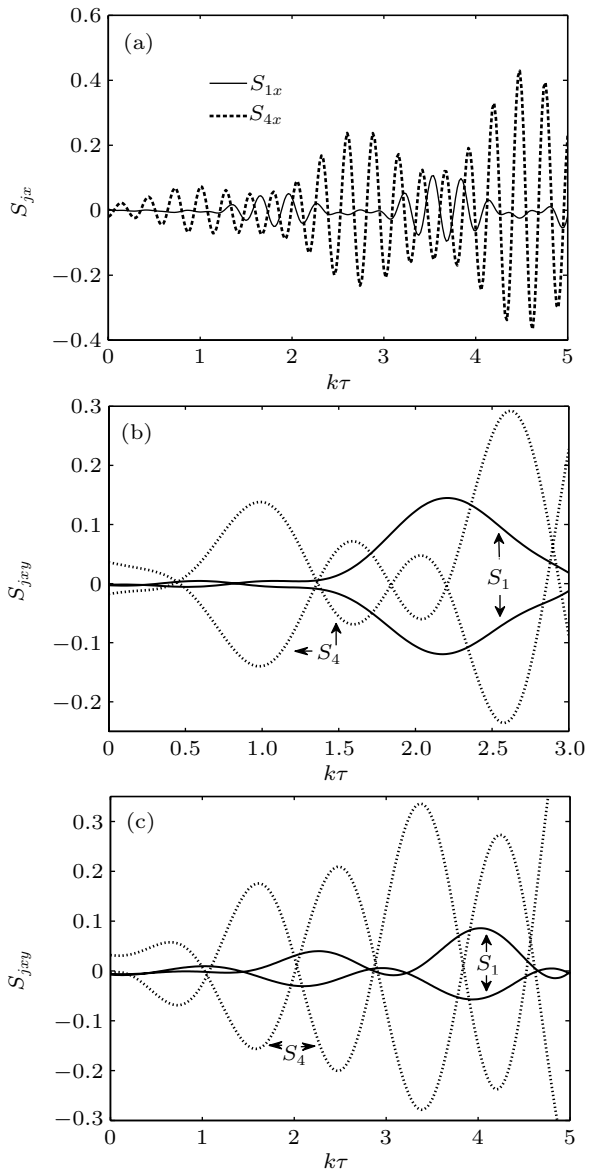


Fig. 7. Comparison of evolution between the single-mode quadrature variance S_{1x}, S_{1y} and four-mode quadrature variance S_{4x}, S_{4y} in the coherent channel α_{c1} at the detuning (a) $\Delta_{js}=10$, (b) $\Delta_{js}=1$, and (c) $\Delta_{js}=0$.

operating frequencies contributes to the generation of enhanced squeezing. In the single-mode basis, the quadrature fluctuation in the X-component is found to be completely below the shot noise level for a certain range, without violating the uncertainty principle. At $\Delta_{js}=1$ squeezing does not need to alternatingly appear between the two quadrature components to complete the period of oscillation. The outcome is essential in a sense that the practical application of squeezed light requires exact prediction of when the squeezing will appear. In such a case, one can be certain that the X-component will exhibit squeezing at specific time interval corresponding to $\Delta_{js}=0$. On the other hand, the result corresponding to four-mode squeezing suggests that quadrature variances may exhibit squeezing in both the quadrature components and the quadrature transition happens at every half-period of their os-

cillation with equal noise distribution. Finally, the squeezing spectrum corresponding to the four-mode basis shows a stronger squeezing than that in the case of single-mode one where the maximal noise reduction appears at the longest interaction length.

It should also be noted that a higher number of waveguide channels (following similar configuration) can be employed to extend the non-classical effects. Nevertheless, in the present approach, the mathematical dimension of the system is proportional to the number of interacting modes between the waveguides. A large number of modes results in a higher number of system equations. This requires integration of a larger set of linear equations with noise sources over many trajectories. Here, for example, a minimum of 10^4 trajectories was employed to generate the current results. This requires complex measures and time-consuming computational operations. For this reason, we have limited the number of interacting modes to $n = 4$ in the Hamiltonian given by Eq. (1).

4. Conclusion

Switching properties, photon statistics, and squeezing profiles of the single- and compound-mode intracavity four-channel Kerr NLDC are studied within the approximated solution of Wigner phase-space representation. The abrupt coupling of mean field dynamics is simulated, and the effective transfer of energy across waveguides is discussed under different choices of detuning. In all cases, the mean fields show a strong transition of photon property between the super-Poissonian and sub-Poissonian statistics. The cavity setup, in addition to the multichannel arrangement, allows different types of squeezing to be generated, and enhanced squeezing is obtained for all the considered detuning values. In terms of single-mode squeezing, close to cavity resonance ($\Delta_{js} = 0$), a stronger leaf-revival-collapsed-like squeezing appears as opposed to the system without cavity. Detuning the cavity to $\Delta_{js} = 1$ eliminates the collapsed-and-revival pattern to yield better noise reduction with larger periodic oscillations. The maximum squeezing is found at $\Delta_{js} = 0$. For the case where all vacuum channels are without interaction, the case of $\Delta_{js} = 0$ exhibits maximum squeezing. The enhanced squeezing noticed in the compound-mode for all detuning values indicates that the multichannel system, with the aid of a cavity setup, may be used as a viable source of squeezed light.

References

[1] Moore G E 1965 *Electronics* **38** 114
[2] O' Brien J L 2007 *Science* **318** 1567
[3] Liu N, Thompson J, Weedbrook C, Lloyd S, Vedral V, Gu M and Modi K 2016 *Phys. Rev. A* **93** 052304
[4] Hotta M, Matsumoto J and Yusa G 2014 *Phys. Rev. A* **89** 012311
[5] Aasi J, Abadie J, Abbott B P et al 2013 *Nat. Photon.* **7** 613
[6] Sun H X, Liu K, Zhang J X and Gao J R 2015 *Acta Phys. Sin.* **64** 234210 (in Chinese)
[7] Taylor M A, Janousek J, Daria V, Knittel J, Hage B, Bachor H A and Bowen W P 2014 *Phys. Rev. X* **4** 011017
[8] Zhou B J, Liu X J, Zhou Q P and Liu M W 2007 *Chin. Phys. B* **16** 420
[9] Vahlbruch H, Khalaidovski A, Lastzka N, Gräf C, Danzmann K and Schnabel R 2010 *Class. Quantum Gravity* **27** 084027
[10] Takeno Y, Yukawa M, Yonezawa H and Furusawa A 2007 *Opt. Express* **15** 4321
[11] Zhou J, Fan H Y and Song J 2017 *Chin. Phys. B* **26** 070301
[12] Tian J F, Zuo G H, Zhang Y C, Li G, Zhang P F and Zhang T C 2017 *Chin. Phys. B* **26** 124206
[13] Vahlbruch H, Mehmet M, Chelkowski S, Hage B, Franzen A, Lastzka N, Goßler S, Danzmann K and Schnabel R 2008 *Phys. Rev. Lett.* **100** 033602
[14] Zou H M and Fang M F 2016 *Chin. Phys. B* **25** 070305
[15] Zhou B J, Peng Z H, Jia C X, Jiang C L and Liu X J 2014 *Chin. Phys. B* **23** 120305
[16] Zhou B J, Liu X J, Zhou Q P and Liu M W 2007 *Chin. Phys.* **16** 420
[17] Sete A E and Eleuch H 2010 *Phys. Rev. A* **82** 043810
[18] Eleuch H, Courty J M, Messin G, Fabre C and Giacobino E 1999 *J. Opt. B: Quantum SemiClass. Opt.* **1** 1
[19] Eleuch H 2008 *Eur. Phys. J. D* **49** 391
[20] Sete A E and Eleuch H 2014 *Phys. Rev. A* **89** 013841
[21] Qin W 2016 *Chin. Phys. B* **25** 010304
[22] Feng X M, Xioa Y, Yu Y F and Zhang Z M 2015 *Chin. Phys. B* **24** 050301
[23] Mecozzi A 1988 *Opt. Lett.* **13** 925
[24] Podoshvedov S A, Noh J and Kim K 2002 *Opt. Commun.* **212** 115
[25] El-Orany F A A, Perina J and Abdalla M S 2001 *J. Opt. B: Quantum SemiClass. Opt.* **3** 67
[26] Ibrahim A B M A, Umarov B A and Wahiddin M R B 2000 *Phys. Rev. A* **61** 043804
[27] White A G, Lam P K, McClell, D E, Bachor H A and Munro W J 2000 *J. Opt. B: Quantum SemiClass. Opt.* **2** 553
[28] El-Orany F A A, Abdalla M S and Perina J 2005 *Eur. Phys. J. D* **33** 453
[29] Julius R, Ibrahim A B M A, Deni M S M and Umarov B 2013 *AIP Conf. Proc.* February 2013 Kuala Lumpur, Malaysia p. 169
[30] Umarov B A, Ibrahim A B M A and Wahiddin M R B 2001 *Nonlinearity Disorder: Theory Appl.* (Neth.: Springer) p. 341
[31] Bernstein L J 1992 *Opt. Commun.* **94** 406
[32] Bache M, Gaididei Y B and Christiansen P L 2003 *Phys. Rev. A* **67** 043802
[33] Yu L, Li C, Fan J, Chen G, Zhang T C and Jia S 2016 *Chin. Phys. B* **25** 050301
[34] Mallon, Reid M D and Olsen M K 2008 *J. Phys. B: At. Mol. Opt. Phys.* **41** 015501
[35] Midgley S L W, Ferris A J and Olsen M K 1909 arXiv:09064851[quant-ph]
[36] Olsen M K 2006 *Phys. Rev. A* **73** 053806
[37] Nemet N and Parkins S 2016 *Phys. Rev. A* **94** 023809
[38] Julius R, Ibrahim A B M A and Deni M S M 2014 *Laser Phys.* **24** 035202
[39] McCosker R J and Town G E 2010 *J. Sensors Actuators B: Chem.* **150** 417
[40] McCosker R J and Town G E 2010 *Aust. Conf. Opt. Fibre Technol.* December 5–9 2010 Melbourne, Australia, p. 1
[41] McCosker R J 2011 *Design and Applications of Multi-Channel Directional Couplers* (Ph. D. thesis) (Sydney: Macquarie University)
[42] Chianca C V and Olsen M K 2011 *Phys. Rev. A* **83** 043607
[43] Drummond P D and Gardiner C W 1980 *J. Phys. A: Math. Gen.* **13** 2353
[44] Mandel L 1979 *Opt. Lett.* **4** 205
[45] Walls D F and Milburn G J 1994 *Quantum Optics* (Berlin: Springer)
[46] Loudon R and Knight P L 1987 *J. Mod. Opt.* **34** 709